

Lattice Symmetry and Emergence of Antiferromagnetic Quantum Hall States

Morad Ebrahimkhas,^{1,*} Mohsen Hafez-Torbatı,^{2,3,†} and Walter Hofstetter^{2,‡}

¹*Department of Physics, Mahabad Branch, Islamic Azad University, Mahabad, Iran*

²*Institut für Theoretische Physik, Goethe-Universität, 60438 Frankfurt/Main, Germany*

³*Lehrstuhl für Theoretische Physik I, Technische Universität Dortmund, Otto-Hahn-Straße 4, 44221 Dortmund, Germany*

We consider the spinful Harper-Hofstadter model extended by a next-nearest-neighbor (NNN) hopping which opens a gap at half-filling and allows for the realization of a quantum Hall insulator (QHI). The QHI has the Chern number $C = 2$ as both spin components are in the same quantum Hall state. We add to the system a staggered potential Δ along the \hat{x} -direction favoring a normal insulator (NI) and the Hubbard interaction U favoring a Mott insulator (MI). The MI is a Néel antiferromagnet (AF) for small and a stripe AF for large NNN hopping. We investigate the U - Δ phase diagram of the model for both small and large NNN hoppings. We show that while for large NNN hopping there exists a $C = 1$ stripe antiferromagnetic QHI (AFQHI) in the phase diagram, there is no equivalent $C = 1$ Néel AFQHI at the small NNN hopping. We discuss that a $C = 1$ AFQHI can emerge only if the effect of the spin-flip transformation cannot be compensated by a space group operation.

The recent experimental achievements in creation of artificial gauge fields [1, 2] have motivated numerous theoretical studies due to the high degree of control and tunability of parameters in a system of ultracold atoms in optical lattices [3]. Simulating the behavior of charged particles in magnetic fields with ultracold atoms is challenging, as the atoms are neutral and do not respond to magnetic fields. Artificial gauge fields are created by taking advantage of the geometrical phase that arises due to the atom-light interaction [1]. In this way, the Harper-Hofstadter model is realized in optical lattices using the laser-assisted-tunneling [4, 5]. The Haldane model is also implemented using the lattice-shaking technique [6]. Further developments are measuring the Chern number of the Hofstadter bands [7] and the momentum-resolved Berry curvature of the Bloch bands [8].

Feshbach resonances can be used to tune the interaction between ultracold atoms [9]. The effect of interaction on topological systems has become an interesting problem in recent years [10]. In the spinless Haldane model the nearest-neighbor interaction induces a transition from a Chern insulator to a charge ordered MI [11]. In spinful systems the Hubbard interaction can drive a normal insulator (NI) into a quantum Hall [12, 13] or quantum spin Hall insulator [14–17]. Interaction-driven topological transitions are studied also in three-dimensional systems [18, 19]. In SU(3) systems, topological transitions from a magnetic insulator into a quantum Hall insulator (QHI) are reported which have no counterparts in the SU(2) case [20].

In the strong coupling limit the Hubbard interaction favors long-range magnetic order, unless quantum fluctuations are strong enough to stabilize a quantum spin liquid or a valence bond crystal state [21]. This can lead to novel magnetic orders when artificial gauge fields or spin-orbit coupling are present in the system [14, 22–24]. In addition, the competition between the band insulator at weak and the Mott insulator at strong interaction can stabilize novel intermediate phases such as antiferromagnetic QHI (AFQHI) with Chern number $C = 1$ as suggested for the Haldane-Hubbard model [12, 13]. In this phase, one of the spin components is in the quantum Hall state and the other in the normal state.

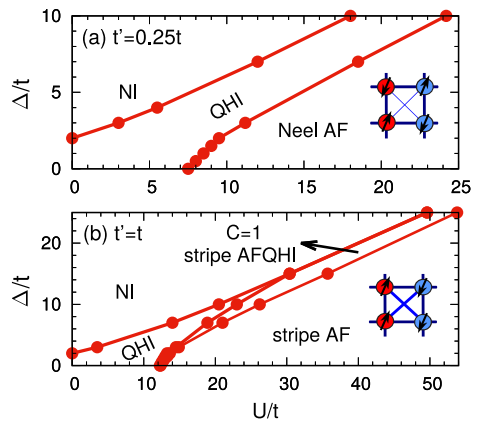


FIG. 1. The phase diagram of the Hamiltonian Eq. (1) for $\varphi = 1/2$ with next-nearest-neighbor hopping $t' = 0.25t$ (a) and $t' = t$ (b). One can identify normal insulator (NI), quantum Hall insulator (QHI), Néel and stripe antiferromagnet (AF), and a $C = 1$ stripe antiferromagnetic QHI (AFQHI) in the phase diagram.

In this work we consider the Harper-Hofstadter-Hubbard model at half-filling with the plaquette flux $1/2$ in units of the magnetic flux quantum h/e . The flux is the same for both spin components. The Harper-Hofstadter model at half-filling is gapless and hence we add a next-nearest-neighbor (NNN) hopping to the system to open a gap and realize a QHI [25]. This QHI has the Chern number $C = 2$. We include also a staggered potential along \hat{x} -direction which favors a NI phase.

We study the phase diagram of the model in the U - Δ plane both for small and for large NNN hopping, in units of nearest-neighbor (NN) hopping t . For small NNN hopping there is a transition from the QHI to the Néel antiferromagnet (AF) upon increasing U for $\Delta < 2t$ as can be seen in Fig. 1(a). For $\Delta > 2t$ the QHI separates the NI at weak from the Néel AF at strong U . For the large NNN hopping in Fig. 1(b) we find that the MI is a stripe AF. An even more interesting difference compared to the small NNN hopping case is the emergence of a $C = 1$ stripe AFQHI in the limit $U \sim 2\Delta \gg t$. We discuss how the compensation of the spin-flip transformation by

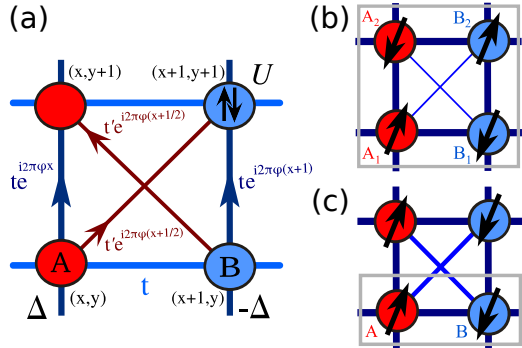


FIG. 2. (a) Schematic representation of the Hamiltonian Eq. (1). Schematic representation of the Néel (b) and the stripe (c) antiferromagnet with the gray box specifying the unit cell.

a lattice translation prevents a $\mathcal{C} = 1$ Néel AFQHI to appear at small NNN hopping. We present results for the spectral function in the bulk and at the edges. We identify gapless edge states for both spin components in the QHI, and gapless edge states for only one spin component in the $\mathcal{C} = 1$ stripe AFQHI phase.

The Hamiltonian of the system reads

$$H = H_t + \Delta \sum_{\vec{r},\sigma} (-1)^x n_{\vec{r},\sigma} + U \sum_{\vec{r}} n_{\vec{r},\downarrow} n_{\vec{r},\uparrow} \quad (1)$$

with the hopping term

$$H_t = - \sum_{\vec{r},\sigma} \left(t c_{\vec{r}+\hat{x},\sigma}^\dagger c_{\vec{r},\sigma} + t e^{2\pi i \varphi x} c_{\vec{r}+\hat{y},\sigma}^\dagger c_{\vec{r},\sigma} + t' \times e^{2\pi i \varphi (x+1/2)} (c_{\vec{r}+\hat{x}+\hat{y},\sigma}^\dagger c_{\vec{r},\sigma} + c_{\vec{r}+\hat{y},\sigma}^\dagger c_{\vec{r}+\hat{x},\sigma}) + \text{H.c.} \right) \quad (2)$$

where t and t' are the NN and the NNN hoppings, respectively. The fermionic operator $c_{\vec{r},\sigma}^\dagger$ ($c_{\vec{r},\sigma}$) creates (annihilates) a particle at position $\vec{r} = x\hat{x} + y\hat{y} = (x, y)$ with spin component $\sigma = \uparrow, \downarrow$. The position \vec{r} runs over the square lattice and the lattice constant is considered as the unit of length. We define the occupation number operator $n_{\vec{r},\sigma} = c_{\vec{r},\sigma}^\dagger c_{\vec{r},\sigma}$. The parameter φ is the magnetic flux entering each plaquette, in units of the magnetic flux quantum. We fix $\varphi = 1/2$. The second term in Eq. (1) is a staggered potential along \hat{x} -direction, with sublattices A and B acquiring, respectively, the onsite energies $+\Delta$ and $-\Delta$. The last term is the Hubbard interaction. The Hamiltonian is schematically depicted in Fig. 2(a). For $U = 0$ the Hamiltonian reduces to a two-level problem in momentum space and for finite t' leads to a transition between the QHI and the NI at $\Delta = 2t$ [26]. If there is no flux and no NNN hopping the Hamiltonian reminiscs the ionic Hubbard model with a NI for weak and a Néel AF for strong U . There are suggestions for intermediate phases [27–31].

We employ the real-space dynamical mean-field theory (RDMFT) approach to analyze the phase diagram of the Hamiltonian Eq. (1). The RDMFT was first used to study

thin film geometries consisted of a finite number of coupled layers [32], and since then has been extended, for example, to address disordered systems [26, 33], exotic magnetism [24, 34–36], and topological insulators [14, 20, 37, 38]. The local self-energy in the DMFT method [39] becomes position-dependent in the real-space extension, allowing for an equal-footing treatment of translationally ordered and disordered systems. We use the RDMFT implementation introduced in Ref. 40. We consider 40×40 lattice sizes with periodic boundary conditions (PBC) in both directions unless mentioned otherwise. The inverse temperature is fixed to $\beta = 50/t$, which we expect to represent the ground state properties of the model. We use exact diagonalization (ED) as the impurity solver [39, 41]. Five bath sites are used for the results that we present unless mentioned otherwise. We have checked that the results for different selected points close to the phase transitions are the same as the results obtained using six and seven bath sites.

The Chern number of the interacting system is determined using the topological Hamiltonian method [42], which relates the Chern number of an interacting system to the Chern number of an effective non-interacting model. The method relies on the adiabatic deformation of the Green's function such that the single-particle gap never closes, leaving the Chern number of the system unchanged. The effective non-interacting model, called topological Hamiltonian, in the Bloch form reads

$$\mathbf{h}_{\text{top}}(\vec{k}) = \mathbf{h}_0(\vec{k}) + \Sigma(\vec{k}, \omega = 0), \quad (3)$$

where $\mathbf{h}_0(\vec{k})$ describes the non-interacting part of the model and $\Sigma(\vec{k}, \omega)$ is the self-energy. In the DMFT method the self-energy is local and hence its role in the topological Hamiltonian Eq. (3) is just to modify the onsite energies. We find that the real part of the self-energy at the smallest, in the absolute value, Matsubara frequency accurately describes the zero-frequency self-energy obtained using a polynomial fit.

We present results first for the small $t' = 0.25t$ and then for the large $t' = t$ NNN hopping. We avoid the intermediate values $0.6t \lesssim t' \lesssim 0.8t$ where in the large- U limit a quantum spin liquid [43–45] or a valence bond crystal [45–48] is expected, which can not be captured within our local self-energy approximation. For $t' = 0.25t$ in Figs. 3(a) and 3(b) we have plotted the local moment $M_{\vec{r}} = |\langle n_{\vec{r},\uparrow} - n_{\vec{r},\downarrow} \rangle|/2$ and the double occupancy $D_{\vec{r}} = \langle n_{\vec{r},\uparrow} n_{\vec{r},\downarrow} \rangle$ versus the Hubbard U for different values of the staggered potential Δ . The local moment is position-independent, $M_{\vec{r}} = M$, and we have plotted the double occupancy on sublattice B , shown as D_B . One can identify a transition between a paramagnetic and a magnetic phase, which is shifted to larger values of U as Δ is increased. The paramagnetic phase can be a NI or a QHI, depending on the value of the Chern number \mathcal{C} . The magnetic phase is a Néel AF denoted schematically in Fig. 2(b).

To determine the topological properties of the system in the paramagnetic and in the magnetic region we analyze the topological Hamiltonian. There are four sites in the unit cell la-

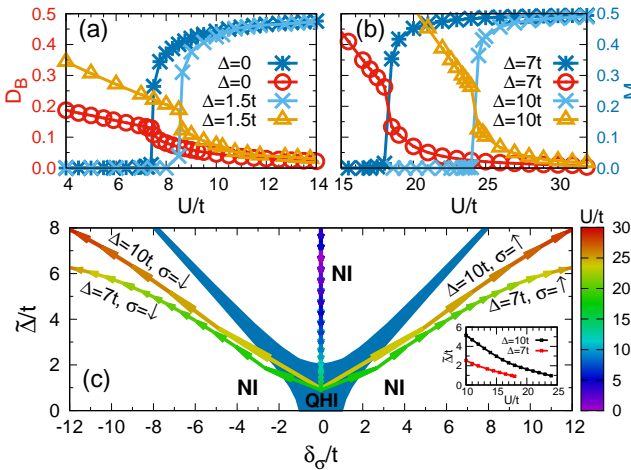


FIG. 3. (a,b) The local moment M and the double occupancy D_B on sublattice B plotted versus the Hubbard interaction U for different values of the staggered potential Δ . (c) The evolution of the effective potentials $\tilde{\Delta}$ and δ_σ upon increasing U for $\Delta = 7t$ and $\Delta = 10t$. Here the color indicates the value of U (see the color-bar). The shaded area indicates a quantum Hall insulator (QHI) and the white area a normal insulator (NI). The inset shows $\tilde{\Delta}$ versus U in the paramagnetic region where $\delta_\sigma = 0$. The results are for the next-nearest-neighbor hopping $t' = 0.25t$.

beled as A_1 , A_2 , B_1 , and B_2 in Fig. 2(b). The topological Hamiltonian, in the second quantization form, up to an irrelevant constant can be written as

$$H_{\text{top}} = H_t + \sum_{\vec{r}, \sigma} \left(\tilde{\Delta}(-1)^x + \delta_\sigma(-1)^{x+y} \right) n_{\vec{r}, \sigma} \quad (4)$$

where H_t is the hopping term Eq. (2) and the effective potentials $\tilde{\Delta}$ and δ_σ are given by

$$\tilde{\Delta} = \Delta + \frac{1}{4} (\Sigma_{A_1}^\sigma(0) + \Sigma_{A_2}^\sigma(0) - \Sigma_{B_1}^\sigma(0) - \Sigma_{B_2}^\sigma(0)), \quad (5a)$$

$$\delta_\sigma = \frac{1}{4} (\Sigma_{A_1}^\sigma(0) - \Sigma_{A_2}^\sigma(0) - \Sigma_{B_1}^\sigma(0) + \Sigma_{B_2}^\sigma(0)), \quad (5b)$$

where $\Sigma_X^\sigma(0)$ is the zero-frequency self-energy at the site X with spin σ . The potential $\tilde{\Delta}$ is spin-independent and $\delta_\uparrow = -\delta_\downarrow$ [49].

The evolution of the effective potentials $\tilde{\Delta}$ and δ_σ upon increasing U for $\Delta = 7t$ and $\Delta = 10t$ is displayed in Fig. 3(c). The shaded area in this figure indicates a QHI and the white area a NI. One can see how upon increasing U the effective potential $\tilde{\Delta}$ is renormalized and the system enters the QHI phase. The inset in Fig. 3(c) displays $\tilde{\Delta}$ versus U in the paramagnetic region where $\delta_\sigma = 0$. Upon entering the magnetic phase the effective potential δ_σ becomes finite and both spin components fall out of the QHI region [50]. This demonstrates that the Néel AF is topologically trivial.

It is apparent from Eq. (4) that the two spin components are always in the same topological state due to $\delta_\uparrow = -\delta_\downarrow$. This makes the emergence of a $\mathcal{C} = 1$ Néel AF impossible. This

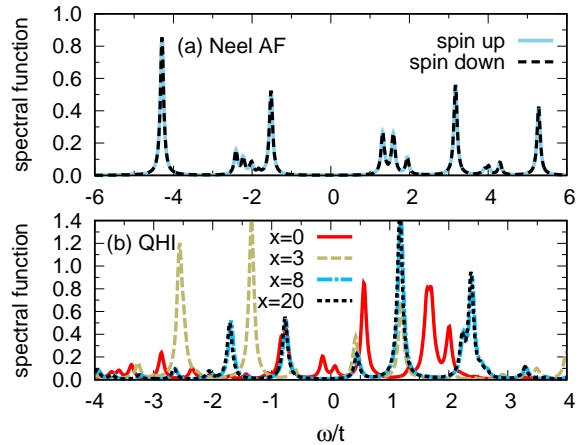


FIG. 4. (a) The bulk spectral function averaged over the sites in the unit cell for up and down spin in the Néel antiferromagnet (AF) with $\Delta = 7t$ and $U = 20t$. (b) The spectral function plotted for different values of x in the quantum Hall insulator (QHI) with $\Delta = 7t$ and $U = 15t$ obtained using a cylindrical geometry with edges at $x = 0$ and $x = 40$. The results are for the next-nearest-neighbor hopping $t' = 0.25t$.

can also be understood from the symmetry of the phase, without considering the topological Hamiltonian Eq. (4). In the Néel AF illustrated in Fig. 2(b) the effect of the spin-flip transformation can be compensated by a lattice translation, i.e., by a shift by one lattice site along \hat{y} -direction. This suggests that spin up and spin down fermion dispersions will differ at most by a shift in momentum space. This is confirmed in Fig. 4(a) which shows an equal spectral function for up and down spin. The spectral function is plotted for $-6 \leq \omega \leq +6$. The spectral function in Fig. 4(b) is for $\Delta = 7t$ and $U = 15t$ and different values of x on a 41×40 lattice with open boundary conditions (OBC) along \hat{x} and PBC along \hat{y} is displayed in Fig. 4(b). The edges are defined at $x = 0$ and $x = 40$ and the lattice is symmetric with respect to the center $x = 20$. Six bath sites are used in the impurity problem. There are gapless excitations at the edge which quickly disappear upon approaching the bulk, consistent with the topological Hamiltonian prediction on a QHI phase.

We consider now the large NNN hopping $t' = t$. The MI phase in this case is a stripe AF with antiferromagnetic ordering along \hat{x} and the ferromagnetic ordering along \hat{y} , see Fig. 2(c). This is due to the finite staggered potential Δ which induces a stronger NN spin exchange coupling along \hat{x} , $J_1^x = 4t^2U/(U^2 - 4\Delta^2)$, than the \hat{y} direction, $J_1^y = 4t^2/U$, in the Mott regime. There are two sites in the unit cell and the topological Hamiltonian for $t' = t$ can be expressed, up to an

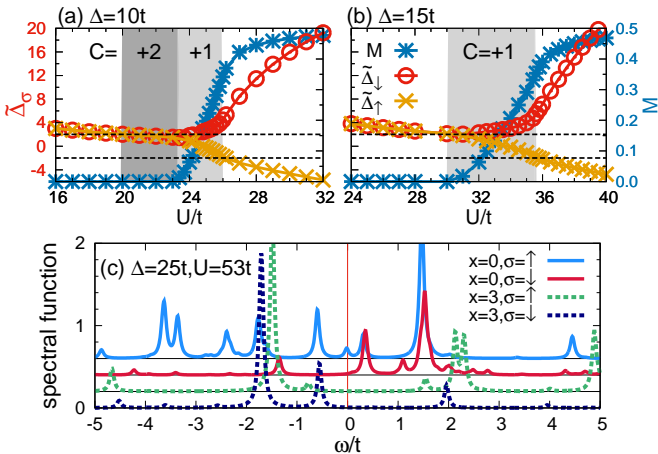


FIG. 5. The local moment M and the effective potential $\tilde{\Delta}_\sigma$ plotted versus the Hubbard interaction U for $\Delta = 10t$ (a) and $\Delta = 15t$ (b). A shaded area indicates a phase with a finite Chern number C . (c) The edge spectral functions for up and down spin in the $C = 1$ stripe antiferromagnetic quantum Hall insulator with $\Delta = 25t$ and $U = 53t$, obtained using a cylindrical geometry with edges at $x = 0$ and $x = 40$. The shift of the spectral function along the vertical axis is for clarity. The results are for the next-nearest-neighbor hopping $t' = t$.

irrelevant constant, as

$$H_{\text{top}} = H_t + \sum_{\vec{r},\sigma} \tilde{\Delta}_\sigma (-1)^x n_{\vec{r},\sigma}, \quad (6)$$

with the effective potential

$$\tilde{\Delta}_\sigma = \Delta + \frac{1}{2} (\Sigma_A^\sigma(0) - \Sigma_B^\sigma(0)), \quad (7)$$

The spin-dependence of this effective potential allows different spin components to fall in different topological regions and consequently a $C = 1$ AFQHI to emerge. The spin component σ is in the quantum Hall state if $|\tilde{\Delta}_\sigma| < 2t$ and in the normal state if $|\tilde{\Delta}_\sigma| > 2t$.

In Figs. 5(a) and 5(b) we have plotted the local moment M and the effective potential $\tilde{\Delta}_\sigma$ versus U for $\Delta = 10t$ (a) and $\Delta = 15t$ (b). The dashed lines at $\tilde{\Delta}_\sigma = 2t$ and $\tilde{\Delta}_\sigma = -2t$ specify the borders of the topological region $|\tilde{\Delta}_\sigma| < 2t$. A shaded area indicates a phase with a finite Chern number C . One can see from Fig. 5(a) that upon increasing U the effective potential $\tilde{\Delta}_\sigma$ drops below $2t$ at $U \simeq 20t$ and a transition from a NI to a QHI takes place. For $U \gtrsim 23t$ the local moment becomes finite and $\tilde{\Delta}_\sigma$ becomes spin-dependent. One spin component, spin down in the figure, almost immediately leaves the topological region while the other spin component remains topological up to $U \simeq 26t$ [51]. This leads to a $C = 1$ stripe AFQHI phase for $23t \lesssim U \lesssim 26t$. Beyond $U \simeq 26t$ the system is a (topologically trivial) stripe AF. One can see from Fig. 5(b) that upon increasing Δ to $15t$ the QHI phase disappears and there is only the $C = 1$ stripe AFQHI between the NI and the stripe AF.

In the stripe AF displayed in Fig. 2(c) the effect of the spin-flip transformation, unlike the Néel AF, can not be compensated by a lattice translation. This leads to a spin-dependent spectral function [49]. This allows up and down spin components to change their Chern numbers at different transition points and the $C = 1$ stripe AFQHI to emerge.

In Fig. 5(c) we have plotted the spectral function near the edge $x = 0$ of a 41×40 cylindrical geometry with $\Delta = 25t$ and $U = 53t$, where the system is expected to be a $C = 1$ stripe AFQHI according to the topological Hamiltonian. The shift of the spectral function along the vertical axis is for clarity. Six bath sites are used in the impurity problem. There are contributions out of the plotted region $-5t \leq \omega \leq +5t$ which mainly belong to the spin down spectral function. Edge excitations in an interacting QHI have been discussed using ED on finite clusters [11] and using RDMFT with ED [20] and with the quantum Monte Carlo [14] impurity solver. We are not aware of a study of edge excitations in an interacting $C = 1$ AFQHI. Although our results in Fig. 5(c) are obtained using a finite number of bath sites and indicate only the qualitative shape of the spectral function, they can still capture the main expected feature that edge excitations are gapless for one spin component and gapped for the other. The edge excitations in optical lattices can be investigated by introducing a Hofstadter interface [37].

To summarize, we compare in Fig. 1 the U - Δ phase diagram of the model Eq. (1) for small $t' = 0.25t$ (a) and large $t' = t$ (b) NNN hopping. Apart from the type of magnetic order, there is a fundamental difference between the two phase diagrams: In Fig. 1(b) there exists an intermediate $C = 1$ stripe AFQHI while in Fig. 1(a) never a $C = 1$ Néel AFQHI appears. The possibility to compensate the effect of the spin-flip transformation on an electronic state with a space group operation suggests an equal single-particle gap for up and down spins. This prevents the spin components from changing their Chern numbers at different transition points and a $C = 1$ AFQHI from emerging.

We notice that our conclusion on the possible existence of a $C = 1$ AFQHI is based on the symmetry of the phase and not the details of the model studied in this paper. For example, replacing the staggered potential along \hat{x} in Eq. (1) with the staggered potential $H_\Delta = \sum_{\vec{r},\sigma} \Delta (-1)^{x+y} n_{\vec{r},\sigma}$ changing along both \hat{x} and \hat{y} directions would lead to the opposite situation, i.e., would allow a $C = 1$ Néel and prevent a $C = 1$ stripe AFQHI. Our conclusion is consistent with the realization of the $C = 1$ AFQHI in the Haldane-Hubbard model [12, 13]. Our results can be used as a guideline for future experiments, especially in optical lattices, searching for AFQHI phases.

We would like to thank Amir A. Ahmad, B. Irsigler, G.S. Uhrig, and J.-H. Zheng for useful discussions. We are indebted to A. Amaricci for reading the initial version of the manuscript and providing helpful comments. This work was supported by the Deutsche Forschungsgemeinschaft (DFG, German Research Foundation) via Research Unit FOR 2414 under Project No. 277974659 (M.H.-T. and W.H.). This work was also supported by the DFG via the high performance com-

puting center LOEWE-CSC. This study has also been supported financially by the German Research Foundation (DFG) and the Russian Foundation for Basic Research (RFBR) in the International Collaborative Research Centre TRR 160, project B8 (M.H.-T.).

* ebrahimkhas@iau-mahabad.ac.ir

† mohsen.hafez@tu-dortmund.de

‡ hofstett@physik.uni-frankfurt.de

[1] N. R. Cooper, J. Dalibard, and I. B. Spielman, *Rev. Mod. Phys.* **91**, 015005 (2019).

[2] M. Aidelsburger, S. Nascimbene, and N. Goldman, *Comptes Rendus Physique* **19**, 394432 (2018), quantum simulation / Simulation quantique.

[3] W. Hofstetter and T. Qin, *Journal of Physics B: Atomic, Molecular and Optical Physics* **51**, 082001 (2018).

[4] M. Aidelsburger, M. Atala, M. Lohse, J. T. Barreiro, B. Paredes, and I. Bloch, *Phys. Rev. Lett.* **111**, 185301 (2013).

[5] H. Miyake, G. A. Siviloglou, C. J. Kennedy, W. C. Burton, and W. Ketterle, *Phys. Rev. Lett.* **111**, 185302 (2013).

[6] G. Jotzu, M. Messer, R. Desbuquois, M. Lebrat, T. Uehlinger, D. Greif, and T. Esslinger, *Nature* **515**, 237 (2014).

[7] M. Aidelsburger, M. Lohse, C. Schweizer, M. Atala, J. T. Barreiro, S. Nascimbne, N. R. Cooper, I. Bloch, and N. Goldman, *Nature Physics* **11**, 162 (2014).

[8] N. Fläschner, B. S. Rem, M. Tarnowski, D. Vogel, D.-S. Lühmann, K. Sengstock, and C. Weitenberg, *Science* **352**, 1091 (2016).

[9] I. Bloch, J. Dalibard, and W. Zwerger, *Rev. Mod. Phys.* **80**, 885 (2008).

[10] S. Rachel, *Reports on Progress in Physics* **81**, 116501 (2018).

[11] C. N. Varney, K. Sun, M. Rigol, and V. Galitski, *Phys. Rev. B* **82**, 115125 (2010).

[12] J. He, Y.-H. Zong, S.-P. Kou, Y. Liang, and S. Feng, *Phys. Rev. B* **84**, 035127 (2011).

[13] T. I. Vanhala, T. Siro, L. Liang, M. Troyer, A. Harju, and P. Trm, *Phys. Rev. Lett.* **116**, 225305 (2016).

[14] D. Cocks, P. P. Orth, S. Rachel, M. Buchhold, K. Le Hur, and W. Hofstetter, *Phys. Rev. Lett.* **109**, 205303 (2012).

[15] J. C. Budich, B. Trauzettel, and G. Sangiovanni, *Phys. Rev. B* **87**, 235104 (2013).

[16] A. Amaricci, J. C. Budich, M. Capone, B. Trauzettel, and G. Sangiovanni, *Phys. Rev. Lett.* **114**, 185701 (2015).

[17] K. Jiang, S. Zhou, X. Dai, and Z. Wang, *Phys. Rev. Lett.* **120**, 157205 (2018).

[18] Amaricci A., Budich J. C., Capone M., Trauzettel B., and Sangiovanni G., *Phys. Rev. B* **93**, 235112 (2016).

[19] B. Irsigler, J.-H. Zheng, F. Grusdt, and W. Hofstetter, *Phys. Rev. Research* **2**, 013299 (2020).

[20] M. Hafez-Torbat, J.-H. Zheng, B. Irsigler, and W. Hofstetter, (2019), [arXiv:1911.03518 \[cond-mat.str-el\]](https://arxiv.org/abs/1911.03518).

[21] L. Balents, *Nature* **464**, 199208 (2010).

[22] J. Radić, A. Di Ciolo, K. Sun, and V. Galitski, *Phys. Rev. Lett.* **109**, 085303 (2012).

[23] V. S. Arun, R. Sohal, C. Hickey, and A. Paramekanti, *Phys. Rev. B* **93**, 115110 (2016).

[24] B. Irsigler, J.-H. Zheng, M. Hafez-Torbat, and W. Hofstetter, *Phys. Rev. A* **99**, 043628 (2019).

[25] Y. Hatsugai and M. Kohmoto, *Phys. Rev. B* **42**, 8282 (1990).

[26] J.-H. Zheng, T. Qin, and W. Hofstetter, *Phys. Rev. B* **99**, 125138 (2019).

[27] M. Hafez-Torbat and G. S. Uhrig, *Phys. Rev. B* **93**, 195128 (2016).

[28] S. S. Kancharla and E. Dagotto, *Phys. Rev. Lett.* **98**, 016402 (2007).

[29] N. Paris, K. Bouadim, F. Hbert, G. G. Batrouni, and R. T. Scalettar, *Phys. Rev. Lett.* **98**, 046403 (2007).

[30] M. Ebrahimkhas, *Physics Letters A* **375**, 32233227 (2011).

[31] A. Shahbazy and M. Ebrahimkhas, *Chinese Journal of Physics* **58**, 273279 (2019).

[32] M. Potthoff and W. Nolting, *Phys. Rev. B* **59**, 2549 (1999).

[33] Y. Song, R. Wortis, and W. A. Atkinson, *Phys. Rev. B* **77**, 054202 (2008).

[34] P. P. Orth, D. Cocks, S. Rachel, M. Buchhold, K. L. Hur, and W. Hofstetter, *Journal of Physics B: Atomic, Molecular and Optical Physics* **46**, 134004 (2013).

[35] M. Hafez-Torbat and W. Hofstetter, *Phys. Rev. B* **100**, 035133 (2019).

[36] Valli Angelo, Amaricci Adriano, Brosco Valentina, and Capone Massimo, *Nano Letters* **18**, 21582164 (2018).

[37] B. Irsigler, J.-H. Zheng, and W. Hofstetter, *Phys. Rev. Lett.* **122**, 010406 (2019).

[38] A. Amaricci, A. Valli, G. Sangiovanni, B. Trauzettel, and M. Capone, *Phys. Rev. B* **98**, 045133 (2018).

[39] A. Georges, G. Kotliar, W. Krauth, and M. J. Rozenberg, *Rev. Mod. Phys.* **68**, 13 (1996).

[40] M. Hafez-Torbat and W. Hofstetter, *Phys. Rev. B* **98**, 245131 (2018).

[41] M. Caffarel and W. Krauth, *Phys. Rev. Lett.* **72**, 1545 (1994).

[42] Z. Wang and S.-C. Zhang, *Phys. Rev. X* **2**, 031008 (2012).

[43] H.-C. Jiang, H. Yao, and L. Balents, *Phys. Rev. B* **86**, 024424 (2012).

[44] W.-J. Hu, F. Becca, A. Parola, and S. Sorella, *Phys. Rev. B* **88**, 060402 (2013).

[45] D. Poilblanc, M. Mambrini, and S. Capponi, *SciPost Phys.* **7**, 41 (2019).

[46] R. Haghshenas and D. N. Sheng, *Phys. Rev. B* **97**, 174408 (2018).

[47] L. Wang, Z.-C. Gu, F. Verstraete, and X.-G. Wen, *Phys. Rev. B* **94**, 075143 (2016).

[48] L. Capriotti and S. Sorella, *Phys. Rev. Lett.* **84**, 3173 (2000).

[49] See Supplemental Materials.

[50] A continuous evolution of the effective potentials in Fig. 3(c) across the magnetic transition implies an intermediate $\mathcal{C} = 2$ Neel AF to exist. However, this region is so narrow that we could not get any converged RDMFT data within it.

[51] There is a narrow region between the QHI and the $\mathcal{C} = 1$ stripe AFQHI where both spin components are in the topological state. This phase is not specified in the figure as it is very narrow, $\simeq 0.5t$, and may not survive beyond the DMFT approximation.

SUPPLEMENTAL MATERIALS

Topological Hamiltonian for small next-nearest-neighbor hoppings

In this section we derive the topological Hamiltonian Eq. (4), which is valid for small next-nearest-neighbor (NNN) hoppings, i.e., for the case that in the large- U limit the system exhibits a Néel antiferromagnet (AF). In general, there are four sites in the unit cell as shown in Fig. 2(b). A local self-energy in Eq. (3) leaves the hopping part of the non-interacting Hamiltonian unchanged and modifies only the on-site energies. One finds

$$\varepsilon_{A_1,\sigma} = +\Delta + \Sigma_{A_1}^\sigma(0), \quad (8a)$$

$$\varepsilon_{A_2,\sigma} = +\Delta + \Sigma_{A_2}^\sigma(0), \quad (8b)$$

$$\varepsilon_{B_1,\sigma} = -\Delta + \Sigma_{B_1}^\sigma(0), \quad (8c)$$

$$\varepsilon_{B_2,\sigma} = -\Delta + \Sigma_{B_2}^\sigma(0), \quad (8d)$$

where $\varepsilon_{X,\sigma}$ represents the onsite energy of the topological Hamiltonian at the position X for the spin component σ . As one can see from Fig. 2(b) the Néel AF is invariant under a spin-flip transformation followed by a one-site lattice translation along \hat{y} direction. This implies the symmetry relation

$$\Sigma_{A_1}^\sigma(\omega) = \Sigma_{A_2}^{\bar{\sigma}}(\omega) \quad , \quad \Sigma_{B_1}^\sigma(\omega) = \Sigma_{B_2}^{\bar{\sigma}}(\omega), \quad (9a)$$

where $\bar{\sigma}$ indicates the opposite direction of σ . There is the second symmetry relation

$$\Sigma_{A_1}^\sigma(0) - \Sigma_{A_2}^\sigma(0) = \Sigma_{B_2}^\sigma(0) - \Sigma_{B_1}^\sigma(0), \quad (9b)$$

which we found from our data and is valid only at zero frequency. Eq. (8) can be rewritten as

$$\varepsilon_{A_1,\sigma} = +\Delta + \Sigma_{A_+} + \Sigma_{A_-}^\sigma, \quad (10a)$$

$$\varepsilon_{A_2,\sigma} = +\Delta + \Sigma_{A_+} - \Sigma_{A_-}^\sigma, \quad (10b)$$

$$\varepsilon_{B_1,\sigma} = -\Delta + \Sigma_{B_+} + \Sigma_{B_-}^\sigma, \quad (10c)$$

$$\varepsilon_{B_2,\sigma} = -\Delta + \Sigma_{B_+} - \Sigma_{B_-}^\sigma, \quad (10d)$$

where we have defined

$$\Sigma_{A_+} := \frac{1}{2} (\Sigma_{A_1}^\sigma(0) + \Sigma_{A_2}^\sigma(0)), \quad (11a)$$

$$\Sigma_{A_-}^\sigma := \frac{1}{2} (\Sigma_{A_1}^\sigma(0) - \Sigma_{A_2}^\sigma(0)), \quad (11b)$$

and similarly for Σ_{B_+} and $\Sigma_{B_-}^\sigma$. Σ_{A_+} and Σ_{B_+} are independent from σ , and $\Sigma_{A_-}^\sigma = -\Sigma_{A_-}^{\bar{\sigma}}$ and $\Sigma_{B_-}^\sigma = -\Sigma_{B_-}^{\bar{\sigma}}$ due to the symmetry relation Eq. (9a). The symmetry relation Eq. (9b) implies $\Sigma_{A_-}^\sigma = -\Sigma_{B_-}^\sigma$. By some straightforward manip-

ulation of Eq. (10) we get

$$\varepsilon_{A_1,\sigma} = C + \tilde{\Delta} + \delta_\sigma \quad (12a)$$

$$\varepsilon_{A_2,\sigma} = C + \tilde{\Delta} - \delta_\sigma \quad (12b)$$

$$\varepsilon_{B_1,\sigma} = C - \tilde{\Delta} - \delta_\sigma \quad (12c)$$

$$\varepsilon_{B_2,\sigma} = C - \tilde{\Delta} + \delta_\sigma \quad (12d)$$

where we have defined the common constant $C := (\Sigma_{A_+} + \Sigma_{B_+})/2$ and the effective potentials

$$\tilde{\Delta} := \Delta + \frac{1}{2} (\Sigma_{A_+} - \Sigma_{B_+}), \quad (13a)$$

$$\delta_\sigma := \frac{1}{2} (\Sigma_{A_-}^\sigma - \Sigma_{B_-}^\sigma). \quad (13b)$$

One notices that $\tilde{\Delta}$ is independent from σ and $\delta_\sigma = -\delta_{\bar{\sigma}}$ due to the symmetry relations Eq. (9). This completes the derivation of Eq. (4) with the effective potentials Eq. (5).

Spectral function in the stripe antiferromagnetic phase

In Fig. 6 we have plotted the bulk spectral function averaged over the sites in the unit cell in the stripe antiferromagnet (AF) for up and down spins. The results are for the staggered potential $\Delta = 15t$, the Hubbard interaction $U = 40t$, and the next-nearest-neighbor hopping $t' = t$. In contrast to the spectral function in the Néel AF in Fig. 4(a) in the main text, the spectral function in the stripe AF depends on spin. This is due to the fact that the effect of the spin-flip transformation can not be compensated by a space group operation in the stripe AF, see Fig. 2(c) in the main text.

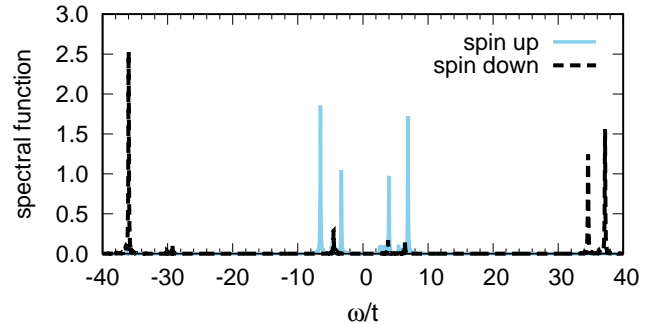


FIG. 6. The spectral function in the stripe antiferromagnetic phase for up and down spins plotted versus the frequency ω . The results are for the staggered potential $\Delta = 15t$, the Hubbard interaction $U = 40t$, and the next-nearest-neighbor hopping $t' = t$.